SCIENTIFIC REPORTS

OPEN

SUBJECT AREAS:
CNS CANCER
CANCER IMAGING
DRUG DEVELOPMENT
PRE-CLINICAL STUDIES

Received
1 July 2013

Accepted
23 August 2013

Published
4 October 2013

Correspondence and requests for materials should be addressed to N.Y.R.A. (Nathalie_Agar@dfci.harvard.edu) or C.D.S. (Charles_Stiles@dfci.harvard.edu)

Molecular imaging of drug transit through the blood-brain barrier with MALDI mass spectrometry imaging

Xiaohui Liu[1], Jennifer L. Ide[1], Isaiah Norton[1], Mark A. Marchionni[2], Maritza C. Ebling[1], Lan Y. Wang[2], Erin Davis[2], Claire M. Sauvageot[2], Santosh Kesari[3], Katherine A. Kellersberger[4], Michael L. Easterling[4], Sandro Santagata[5], Darrin D. Stuart[6], John Alberta[2], Jeffrey N. Agar[7], Charles D. Stiles[2] & Nathalie Y. R. Agar[1,2,8]

[1]Department of Neurosurgery, Brigham and Women's Hospital, Harvard Medical School, Boston MA, [2]Department of Cancer Biology, Dana-Farber Cancer Institute, Harvard Medical School, Boston, MA, [3]University of California San Diego, CA, [4]Bruker Daltonics, Billerica MA, [5]Department of Pathology, Brigham and Women's Hospital, Harvard Medical School, Boston MA, [6]Novartis Institutes for BioMedical Research, Emeryville, CA, [7]Brandeis University, Waltham MA, [8]Department of Radiology, Brigham and Women's Hospital, Harvard Medical School, Boston MA.

Drug transit through the blood-brain barrier (BBB) is essential for therapeutic responses in malignant glioma. Conventional methods for assessment of BBB penetrance require synthesis of isotopically labeled drug derivatives. Here, we report a new methodology using matrix assisted laser desorption ionization mass spectrometry imaging (MALDI MSI) to visualize drug penetration in brain tissue without molecular labeling. In studies summarized here, we first validate heme as a simple and robust MALDI MSI marker for the lumen of blood vessels in the brain. We go on to provide three examples of how MALDI MSI can provide chemical and biological insights into BBB penetrance and metabolism of small molecule signal transduction inhibitors in the brain – insights that would be difficult or impossible to extract by use of radiolabeled compounds.

The specialized microvasculature of the postnatal brain acts as a physiological wall restricting the diffusion of molecules and circulating cells between the blood and the central nervous system (CNS). The physiological purpose of this blood-brain barrier (BBB) is to protect the CNS from toxins and pathogens. However, this same selective permeability impedes the delivery of many potentially useful drugs into the interstitial spaces of the brain[1–3]. Accurate determination of the BBB permeability for potential drug candidates is therefore essential in drug discovery programs, both for drugs targeting the CNS as well as for drugs that should remain outside of the nervous system to limit side effects. Drug concentration in cerebrospinal fluid (CSF) is commonly used to estimate drug penetration into the brain. However, the CSF is a specialized fluid produced by the choroid plexus and is not at all representative of the interstitial milieu of the brain[4,5]. Moreover, the choroid plexus is separated from the blood by the choroid epithelium, creating a blood-CSF barrier, which is distinct from the BBB created by the vascular endothelium.

The visualization of drug distribution is typically accomplished by monitoring the distribution of radiolabeled drug derivatives in blood plasma relative to organs and tissues of interest[6,7]. However the genesis of radiolabeled drug derivatives is an expensive process. Moreover, this approach is vulnerable to false negatives (active drug metabolites missing the radiolabel) and false positives (inactive drug metabolites retaining the label)[8]. Computational approaches complemented by microdialysis and other methods have been used to predict and quantify BBB permeability. However, the utility of these methods is limited[9–12].

Matrix-assisted laser desorption/ionization mass spectrometry imaging (MALDI MSI) has been used to image drug molecule and metabolite distributions in tissue sections[13–15]. The only sample preparation required for this label-free approach is matrix deposition. Chemical images can be acquired within minutes to hours depending largely on the targeted spatial resolution. The images of multiple molecules in a given tissue section can be obtained simultaneously using MALDI MSI, allowing for accurate image co-registration.

We show here that multiplex imaging by MALDI MSI can be exploited to determine BBB permeability. By simultaneous imaging of drug and/or drug metabolite together with heme (delineating the lumen of blood vessels

in the brain) a temporal/spatial map of drug transit into the brain parenchyma can be developed. In studies summarized here, we use fluorescence microscopy together with MALDI MSI to validate the concept. Three "case studies" of anti-cancer small molecules with differential BBB permeability are used to illustrate insights into the distribution and metabolism of drugs within the interstitial spaces of the brain that cannot be obtained by other methods.

Results

Validation of heme as a biomarker of vasculature in the brain. Heme, as a cofactor of hemoglobin in red blood cells, is mainly found within the lumen of blood vessels. As shown in **Figure 1**, heme can be used to visualize the lumen of blood vessels in the brain using MALDI MSI. Validation was achieved by showing co-registration of heme with fluorescein (**Fig. 1**) and FITC (**Supplementary Fig. 2**) - two widely accepted fluorescent dyes that do not transit the lumen of blood capillaries[16,17]. Interestingly, a lateral ventricle delineated by fluorescein in both MALDI MSI and fluorescence images is observed with the absence of heme detection (**Fig. 1a**; yellow arrows). This is because the blood-CSF barrier, which is composed of the vasculature around the choroid plexus, is fenestrated and slightly more permeable than the blood-brain barrier, thereby allowing the better transportation of fluorescein from blood into CSF[18].

Regional differences in integrity of the blood-brain barrier revealed by MALDI MSI. BKM120 (Novartis Pharmaceuticals, Basel, Switzerland) is a small molecule inhibitor of pan-class I phosphatidylinositol 3-kinase (PI3K)[19,20]. By multiple methods including tissue distribution of radiolabled derivatives, BKM120 traverses the BBB[21]. Activation of the PI3K signaling axis, either by gain-of-function mutations in PI3K110α or loss-of-function mutations in PTEN, is a common event in high-grade human gliomas[22,23]. For all of these reasons BKM120 is currently in phase II clinical trial for glioblastoma[21].

The permeability of BKM120 through the BBB in mouse brain can be directly visualized using MALDI MSI. For the images shown in **Figure 2**, mice were dosed with BKM120 by oral gavage and sacrificed after 4 hours. Brains were removed, sectioned and imaged by MALDI MS for heme and BKM120 (m/z 411.2 ± 0.1). Overlay images of heme and BKM120 distributions show that a large proportion of the drug signal does not co-localize with heme, suggesting that BKM120 escapes from the brain vasculature and penetrates the brain parenchyma. Notably however, the segregation of BKM120 from heme is not uniform throughout the brain. Rather, regional differences in apparent integrity of the BBB are noted with maximum drug penetrance seen through the plane of the lateral ventricles and in the region of the cerebellum. These regional differences are especially apparent in three-dimensional reconstructions of MALDI MSI images from drug-treated mice (see **Supplementary Video 1**).

Impact of aberrant tumor vasculature revealed by MALDI MSI. RAF265, previously known as CHIR-265 (Novartis Pharmaceuticals, Basel, Switzerland), is a small molecule inhibitor of the RAF serine/threonine protein kinases[24,25]. Recent studies document activating mutations in BRAF as a frequent oncogenic driver event in pediatric low-grade astrocytomas (PLGAs)[26]. Accordingly small molecule RAF inhibitors are plausible therapeutic agents for these tumors. As shown in **Supplementary Figure 4**, RAF265 can suppress the growth of a "genetically relevant" murine model of PLGA that has been transformed by a human BRAF oncogene provided that the cells are implanted subcutaneously. When the tumor cells are implanted stereotactically into the brains of SCID mice, RAF265 has little if any effect on survival.

The differential effect of RAF265 on subcutaneous versus intracranial tumor implants is indicative of limited BBB penetrance. Curiously however, MALDI MSI images at low resolution (100 μm) shows that RAF265 actually accumulates within the intracranial tumor implants (**Fig. 3a** and **Supplementary Video 2**). Higher resolution images are needed to resolve individual capillaries and venules within the brain. When heme and RAF265 are imaged at 25 μm so as to resolve these individual blood vessels, it can be seen that most of the drug is actually sequestered within the lumen of the tumor vasculature together with heme (**Fig. 3d**). Notably, RAF265 does not accumulate within the vasculature of healthy brain (**Fig. 3b**).

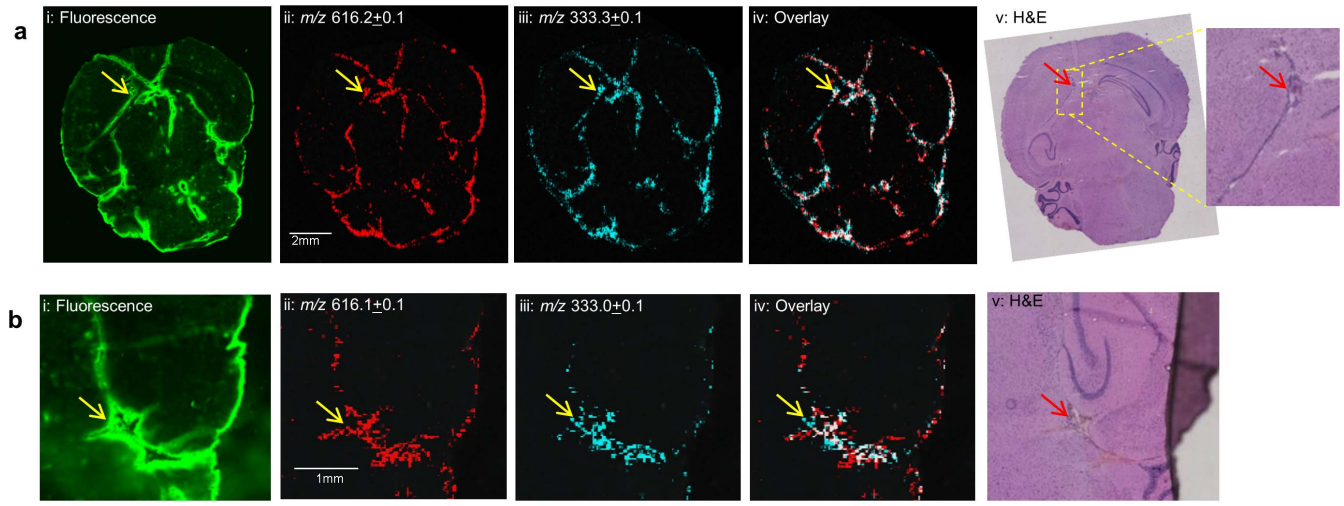

Figure 1 | (a) Comparison of heme and fluorescein images from MALDI TOF MSI at 50 μm resolution with fluorescence image in the same mouse brain section (10 μm thickness) with pre-injected fluorescein. i: fluorescence image of blood vessels from fluorescein (Ex-490 nm, Em-520 nm); ii: heme image (red, m/z 616.2 ± 0.1) from MALDI MSI; iii: fluorescein image (blue, m/z 333.3 ± 0.1) from MALDI MSI (fluorescein spectra presented in **Suppl. Fig. 1**); iv: overlay of heme (red) and fluorescein (blue) from MALDI MSI; v: H&E staining of a sister section from (a) with the expanded view showing the lateral ventricle; The yellow arrow indicates the lateral ventricle delineated by fluorescein with the absence of heme. The red arrow shows blood in the H&E staining image. (b) Selected view of heme and fluorescein images from MALDI MSI under 25 μm resolution and fluorescence image in the same mouse brain section. i: fluorescence image of blood vessels from fluorescein (Ex-490 nm, Em-520 nm); ii: heme image (red, m/z 616.1 ± 0.1) from MALDI MSI; iii: fluorescein image (blue, m/z 333.0 ± 0.1) from MALDI MSI; iv: overlay of heme (red) and fluorescein (blue) from MALDI MSI; v: H&E staining of a sister section. The arrow shows the region of blood.

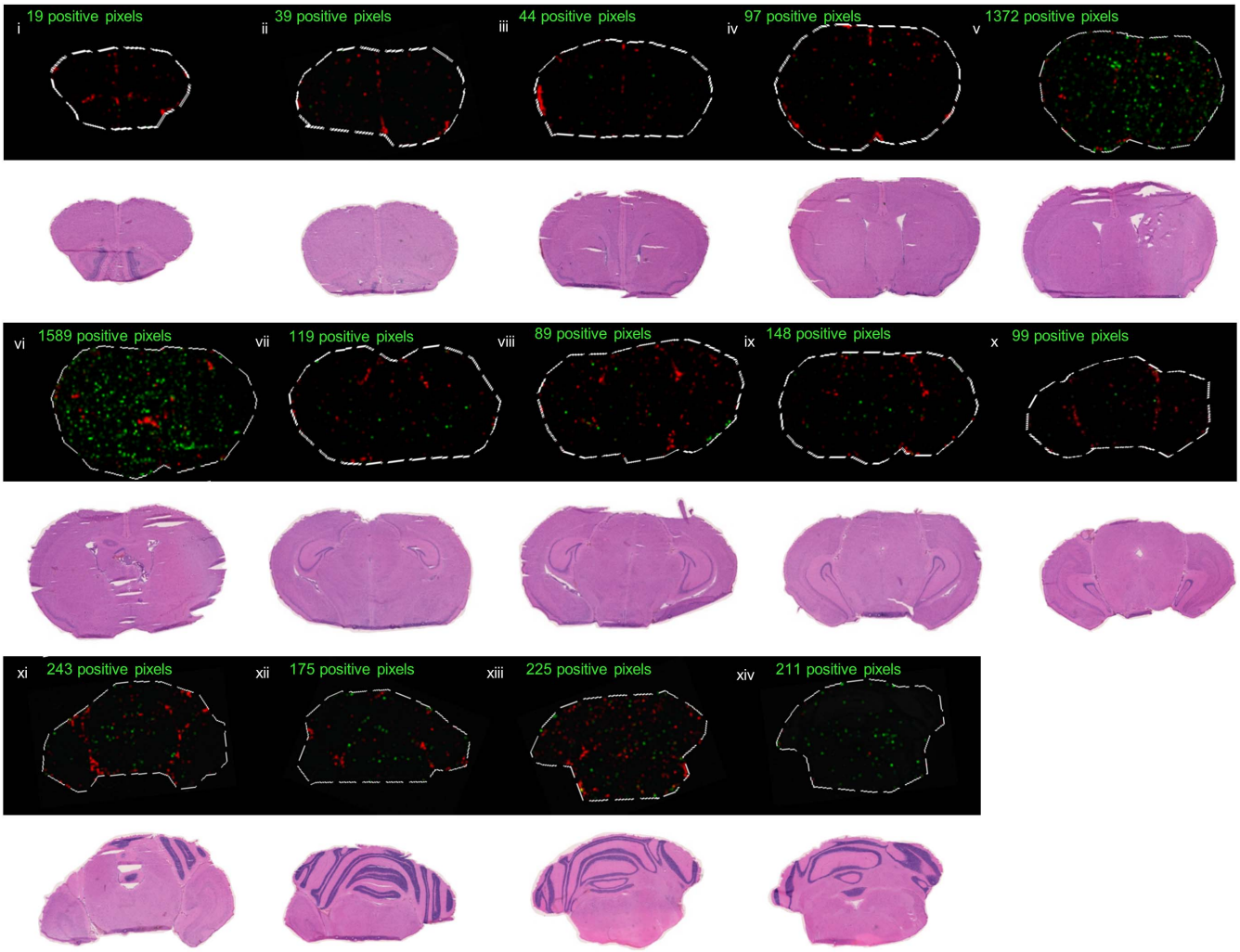

Figure 2 | Overlaid heme (red, *m/z* 616.1 ± 0.1) and BKM120 (green, *m/z* 411.2 ± 0.1) images from MALDI MSI of serial coronal sections of mouse brain at 4-hour dosing time (dosage 200 mg/kg) used to reconstruct the 3D model in Supplementary Video 1. (BKM120 spectra presented in **Suppl. Fig. 3**) H&E staining of sister sections are displayed below. Sections were collected at 500 μm intervals and imaged at 100 μm spatial resolution by MALDI MSI. Regions that show the highest drug diffusion are sections containing the posterior lateral ventricles (v and vi), and near the Circle of Willis in the inferior portion of the brain (xii, xiii, and xiv).

What accounts for the accumulation of RAF265 within the tumor vasculature? Jain and others have noted that the vasculature of many solid tumors is swollen and engorged due to the impact of tumor cytokines such as vascular endothelial growth factor (VEGF), resulting in reduced blood flow at the tumor area[27,28]. Within such a tumor microenvironment, circulating drug molecules are not cleared efficiently, and accumulate within the abnormal blood vessels. In accord with this view immunostaining for blood vessel endothelial cells (using an antibody to CD31 – Cluster of differentiation 31) reveals numerous dilated blood vessels within the intracranial tumor implants (**Fig. 4**).

MALDI FTICR imaging of drug metabolites in brain parenchyma. Erlotinib is a small molecule inhibitor of the epidermal growth factor receptor (EGFR) that is known to be extensively metabolized within the liver[29–34]. As indicated schematically (**Fig. 5**) erlotinib itself and two of its liver metabolites are biologically active; however multiple metabolites of erlotinib are biologically inert. The predicted BBB penetrance of these various metabolites predicated upon molecular mass and hydrophobicity is roughly equivalent. Pharmacologically inactive metabolites such as these could, in principle, confound studies of BBB penetrance using isotopically labeled erlotinib derivatives.

As shown in **Supplementary Figure 6** we can resolve erlotinib and four of its known metabolites from a single 60 μm MALDI Fourier transform ion cyclotron resonance (FTICR) pixel from the liver of a drug treated mouse at 4 hours after drug treatment. The high mass accuracy of FTICR acquisition (<1 ppm mass tolerance) results in confident assignment of the erlotinib (*m/z* 394.17613) and the metabolites. A visual representation of erlotinib and these same four metabolites within the liver of a drug-treated mouse (derived from the data set shown in **Supplementary Fig. 3**) is shown in **Figure 6a**.

The permeability of erlotinib and its metabolites through the blood-brain barrier was investigated in a xenograft mouse model with human U87 glioma cells (**Fig. 6b**). Histopathological evaluation of the tissue sections revealed the tumor margin on serial brain sections (**Fig. 6b**). High intensity heme signal was observed around the tumor margin consistent with local disruption of the blood-tumor barrier and hemorrhage. Erlotinib was observed to be more evenly distributed within as well as at the infiltrative margins of the tumor region and independently of the heme signal (**Fig. 6b**), indicating that the drug molecules escape from the tumor vasculature. As shown in **Figure 6b**, we can also detect one of the erlotinib metabolites (M13/14) within the tumor microenvironment although this metabolite is much less abundant than erlotinib itself. This

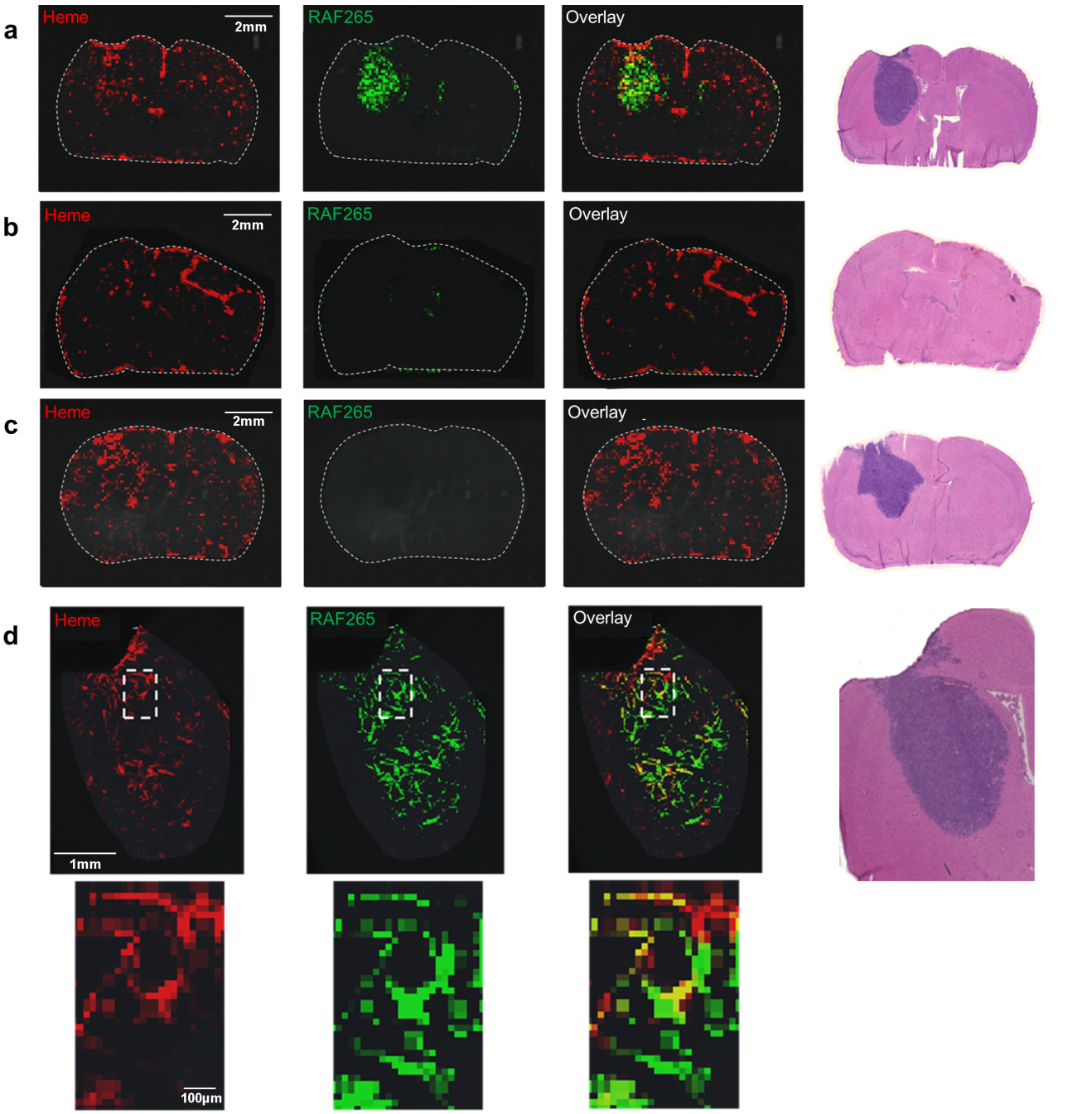

Figure 3 | (a)–(c) MALDI TOF MS images of mouse brain tissue (10 μm thickness) for heme (red, m/z 616.2 ± 0.1) and RAF265 (green, m/z 519.2 ± 0.1) distribution under 100 μm spatial resolution RAF265 spectra presented in **Suppl. Fig. 5**). (a) brain with PVL311 xenograft tumor with a 2-hour single dose of 60 mg/kg RAF265; (b) control healthy brain after 2-hour RAF265 treatment; (c) control brain with PVL311 xenograft tumor but no drug treatment. (d) MALDI TOF MS imaging of selected tumor region under 25 μm spatial resolution. Yellow color indicates overlay of heme and RAF265. H&E staining of sister sections are displayed on the right.

differential abundance of erlotinib relative to M13/14 was also noted in liver (**see Fig. 6a**) and in prior studies by Ling et al[35].

Discussion

An important unmet need in drug development for CNS indications is a method for monitoring drug transit through the BBB that is not dependent upon molecular labeling of drug candidates. We show here that correlation of drug and heme images by MALDI MSI can be used to image drug permeability through the BBB. Moreover, MALDI MSI images reveal insights into other facets of drug delivery into brain and brain tumors that cannot not be obtained by conventional methodology such as i) regional differences in integrity of the BBB, ii) impact of aberrant tumor vasculature on drug penetrance, and iii) resolution of drug and drug metabolites.

The direct imaging of drug penetrance of the BBB by MALDI MSI holds potential in screening for drug candidates targeting the central nervous system, as well as for drugs that should remain outside the central nervous system to minimize side effects. The 3D models reconstructed from MS and optical images provided insight in drug distribution as it relates to brain anatomy. Interestingly, higher concentrations of drugs were observed in the vicinity of the lateral ventricles and the cerebellum for both RAF265 and BKM120. This

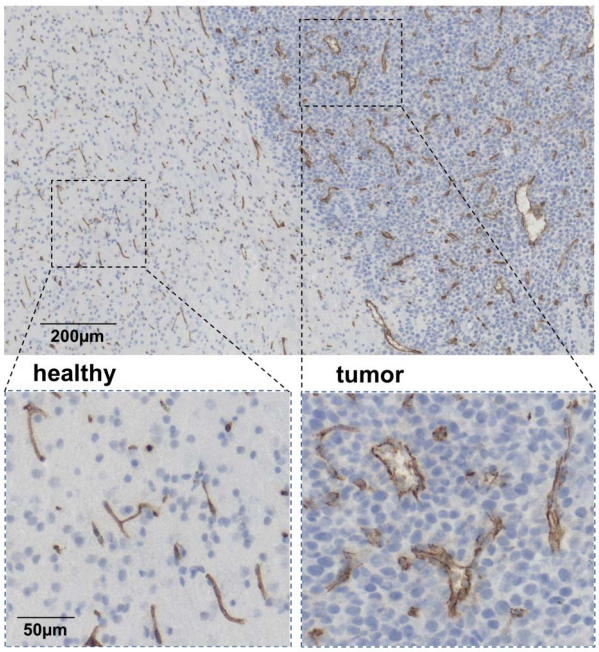

Figure 4 | CD31 staining of blood vessels in mouse brain with PVL311 xenograft tumor. Cluster of differentiation 31 (CD31) antibody staining was applied to stain the normal and abnormal blood vessels in PVL311 tumor. Abnormal blood vessels are swollen and the endothelial cells stained by CD31 in tumor are not well organized as in normal blood vessels in the image.

phenomenon suggests that the therapeutic effect of these drugs on brain tumor may vary depending on tumor location in the brain, and invites for including the consideration of brain anatomy in defining dosing regimens.

MALDI MSI also lends itself to more direct applications in the context of drug development for CNS cancers. For example, the time course of drug transit through the BBB or through the blood-tumor barrier could be imaged in patients undergoing surgery. In the fullness of time, MALDI MSI could move beyond imaging of drugs per se and be used to image the cellular response to targeted therapeutics in the human brain.

Methods

Tissue preparation- healthy mouse brain. Fluorescein and fluorescein 5(6)-isothiocyanate (FITC) were used to validate MALDI MS imaging of mouse brain vasculature using fluorescence microscopy and MALDI MSI. The mice were injected with 400 mg/kg fluorescein sodium salt (Sigma-Aldrich, St. Louis, MO) or FITC (Sigma-Aldrich, St. Louis, MO) in PBS from the tail vein and sacrificed after three minutes. The mouse brain was flash frozen in liquid nitrogen and stored in −80°C freezer. For tissue sectioning, the frozen mouse brain was mounted with minimal amount of optimal cutting medium (OCT) compound, such that OCT did not come into contact with the cryotome blade, and sectioned at 10 μm thickness using a Microm HM550 cryostat (Mikron Instruments Inc, Vista, CA). The specimen temperature was set at −19°C and chamber temperature at −20°C. Tissue sections were thaw-mounted on indium tin oxide (ITO) coated glass slides (BrukerDaltonics, Germany) for mass spectrometry imaging, and sister sections were mounted independently on optical slides (Fisher, Pittsburgh PA) for histochemistry. The slides were first analyzed using fluorescence microscopy, followed by MALDI time-of-flight (TOF) mass spectrometry imaging of the same section.

Tissue preparation- mouse orthotopic models. Human U87- Animal models were prepared by intracranial injections of human U87 glioma cells or murine PVL311 neural stem cells (derived from embryonic brains of p53-null mice and transformed to express human B-RAF V600E point mutation), both lines engineered to

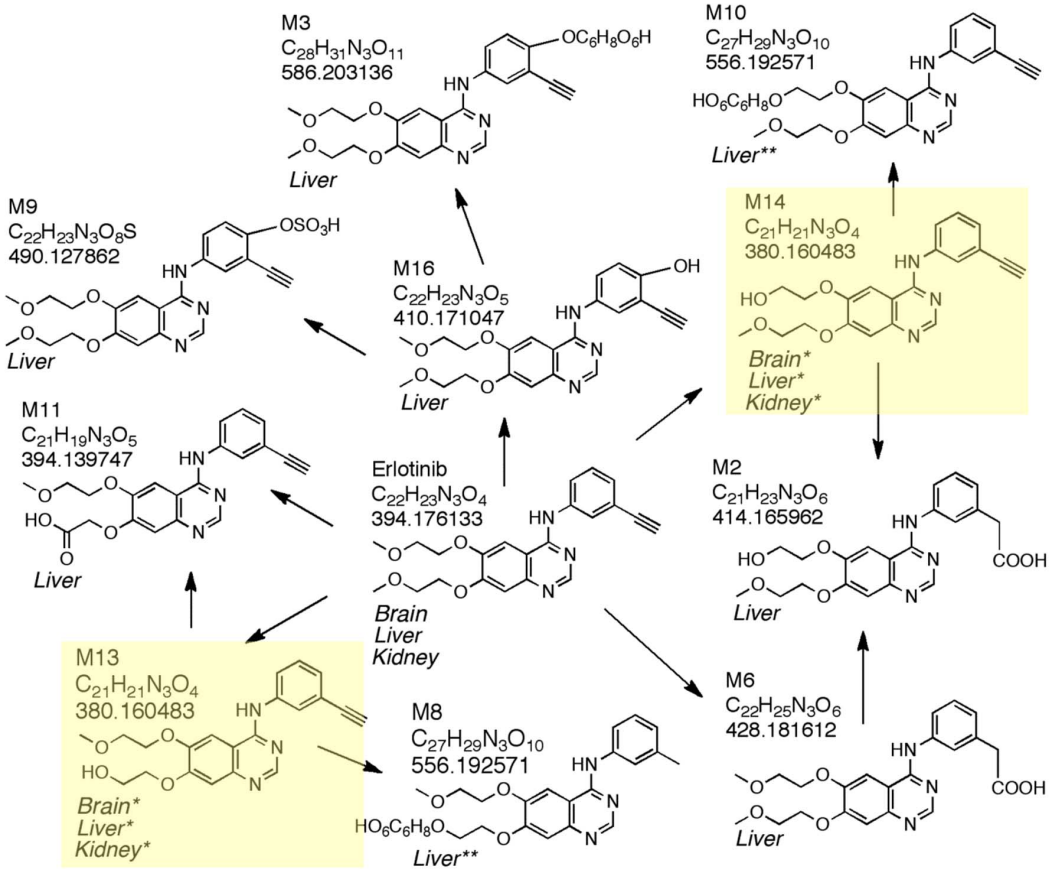

Figure 5 | The structures of erlotinib and its possible metabolites. The chemical compositions and positively charged ion mass are included. The pharmacologically active metabolite M14 and its isomer M13 are highlighted in yellow. Organs in which the metabolites were detected are indicated below each metabolite. In total, 10 metabolites out of the 14 metabolites reported by Ling *et al*[35] were directly detected by MALDI FTICR MSI.

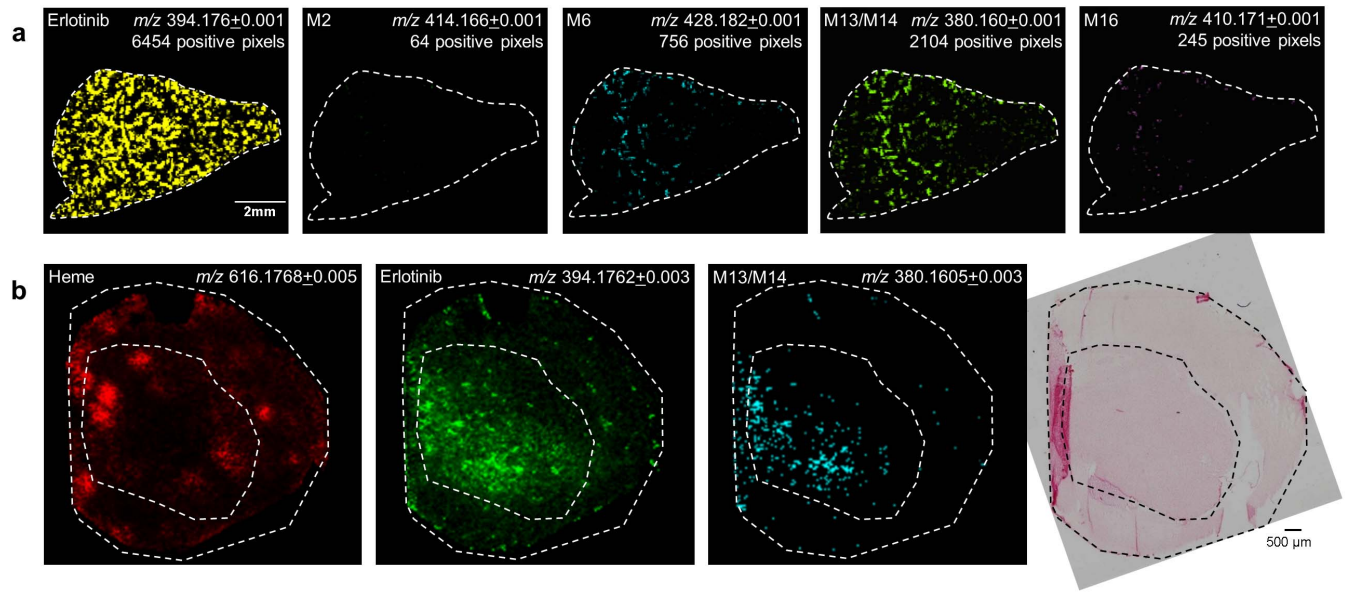

Figure 6 | (a) MALDI FTICR MSI images of different metabolites including M2, M6, M13/14 and M16 from mouse liver treated with erlotinib under 60 µm resolution. (b) Correlation of MALDI FTICR MSI images of heme, erlotinib and metabolite M13/M14 in mouse brain tissue (10 µm thickness) with U87 xenograft tumor. Images were acquired at 50 µm resolution for a total of 14,000 spectra, and sister sections were H&E stained. Heme (red, *m/z* 616.1768 ± 0.005), erlotinib (green, *m/z* 394.1762 ± 0.003), and M13/M14 (light blue, *m/z* 380.1605 ± 0.003). The tissue section is outlined with the exterior dashed line, and the tumor boundaries are outlined by the interior dashed line as determined by a pathologist.

overexpress luciferase. Tumor growth was monitored by *in vivo* bioluminescence imaging, after intra-peritoneal (I.P.) injection of luciferin at 225 mg/kg (mice sedated via inhalation of ~3% isoflurane). The animals were imaged using a CCD camera after 10 minutes. After documentation of tumor growth, the animals were treated by oral gavage of therapeutic levels of drug, and sacrificed at half-point to the *in vivo* half-life of the active compound. The animals were promptly dissected and liver, kidney, and brain were flash frozen in liquid nitrogen. Sections with 10 µm thickness were collected for mass spectrometry and histochemistry analysis. All animal experiments were approved by the Dana Farber Animal Care and Use Committee and distress to animals was minimized. Tissue sections were transferred using a brush onto indium tin oxide (ITO) coated glass slides for mass spectrometry imaging or optical slides for immunohistochemistry and hematoxylin and eosin (H&E) staining.

Matrix preparation. The ImagePrep (BrukerDaltonics, Germany), which can spray matrix solution homogeneously, was used for matrix deposition on ITO coated slides. The matrix solution was 30 mg/mL 2,5-dihydroxybenzoic acid dissolved in 50% HPLC grade methanol, 50% HPLC grade water and 0.2% trifluoroacetic acid. The solution was sonicated for 5 min and centrifuged at 10,000 rpm for 10 min before transferred to the ImagePrep. The ITO coated slides from −80°C freezer were dehydrated in a dessicator for 15 min upon thawing. The matrix was sprayed onto the slides by piezoelectric nebulization in ImagePrep with approximately 85 thin layers of matrix deposition. Chemicals were purchased from Sigma (Sigma-Aldrich, St. Louis, MO).

MALDI TOF mass spectrometry. MALDI TOF imaging was performed using the UltrafleXtreme MALDI TOF/TOF (Bruker Daltonics, Germany) in positive reflectron ion mode with a 1 KHz smartbeam laser. The instrument was calibrated with peptide calibration standard (Bruker Daltonics, Germany) for *m/z* 700–1800. Tissue sections were imaged with spatial resolution from 25–100 µm. Each spectrum was acquired from 200 or 300 laser shots. The MALDI images were displayed using the software FlexImaging 3.0.

MALDI FTICR mass spectrometry. The tissue sections analyzed by MALDI q-FTICR mass spectrometry (Apex-Ultra, Bruker, MA) were imaged with 45 µm to 220 µm laser raster. Instruments with magnetic fields from 7.0–12.0 T were used, with the infinity ion cyclotron resonance cell geometry[36], dual MALDI/electrospray source (Apollo II), and vacuum elements with readings of below 4×10^{-10} mbar in the analyzer region. The instrument was calibrated in ESI mode using 0.01 mg/mL sodium formate (Sigma-Aldrich, St. Louis, MO) solution in 50% acetonitrile 0.1% formic acid. However, the imaging experiment was performed under MALDI mode. Mass spectrometry experiments involved the following steps. Initially MALDI source and transfer parameters were optimized for maximum signal magnitude. Next, excitation amplitude was tuned for maximum accuracy under internal calibration conditions[37]. Sidekick trapping[38] was employed. Chirp excitation and image charge detection was performed. The free induction decay (FID) was multiplied by a sine bell apodization function and was fast Fourier transformed. The mass range for the filters was *m/z* ± 0.001 and the intensity range were 100,000 to 1,000,000 which was set to avoid picking noise signal and was tested in negative controls. The theoretical masses and molecule fine structures were calculated and predicted by a lab-developed software[39].

Fluorescence microscopy. Fluorescence imaging was performed on the same tissue as for MALDI MSI prior to MALDI matrix spraying. Fluorescein and fluorescein isothiocyanate (FITC), two BBB impermeable fluorophores have excitation maximum of 490 nm and 492 nm, and emission maximum at 518 nm and 514 nm respectively. Fluorescence images were acquired using a fluorescent microscope Observer.Z1 with the X-Cite 120Q series light source and AxioCam MRm mounted camera (Zeiss, Germany) with 5× objective, optovar of 1.6, and 1 s exposure time.

Histochemistry. The tissue morphological information was revealed on sister sections of the ones for MS imaging using standard hematoxylin and eosin staining (H&E Staining). All the reagents used for staining were from Sigma (Sigma-Aldrich, St. Louis, MO). After the sections were dried, toluene was applied and the slides and covered with glass coverslips. The optical images of tissues were scanned by Axio Imager M1 microscope (Zeiss, Chester, VA) at 40× magnification. The detailed morphology information of healthy sections and tumors was evaluated on the Mirax Digital Slide Desktop Server system.

Data analysis and 3D reconstruction. For the images obtained from MALDI imaging, heme and various drugs have identical maximum absolute intensity threshold respectively. The minimum intensity threshold is based on examining individual imaging pixels until showing reasonable S/N ratio in spectrum for each image. 3D Doctor is used for 3D reconstruction of MS images and optical images. For RAF265 study, the 3D models of heme, drug and histological images are built individually. However, for BKM120, heme and drug images from the same brain tissue are considered as consecutive sections and reconstructed within one model. In reconstructed models, heme and drug distributions are highlighted using the function of "interactive segment" in 3D Doctor (Able Software Corp., Lexington, MA) without displaying intensity discrepancy. The reconstruction of optical images is based on drawing outlines of regions of interest manually.

1. Chamberlain, M. C. Anticancer therapies and CNS relapse: overcoming blood-brain and blood-cerebrospinal fluid barrier impermeability. *Expert Rev. Neurother.* **10**, 547–561 (2010).
2. Pardridge, W. M. Blood-brain barrier delivery. *Drug Discov. Today* **12**, 54–61 (2007).
3. Deli, M. A., Abraham, C. S., Kataoka, Y. & Niwa, M. Permeability studies on in vitro blood-brain barrier models: physiology, pathology, and pharmacology. *Cell. Mol. Neurobiol.* **25**, 59–127 (2005).
4. Kandel, E. R., Schwartz, J. H. & Jessell, T. *Principles of Neural Science Edn. fourth* (McGraw Hill United States of America; 2000).

5. Hawkins, B. T. & Davis, T. P. The blood-brain barrier/neurovascular unit in health and disease. *Pharmacol. Rev.* **57**, 173–185 (2005).
6. Solon, E. G., Balani, S. K. & Lee, F. W. Whole-body autoradiography in drug discovery. *Curr. Drug Metab.* **3**, 451–462 (2002).
7. Solon, E. G., Schweitzer, A., Stoeckli, M. & Prideaux, B. Autoradiography, MALDI-MS, and SIMS-MS imaging in pharmaceutical discovery and development. *AAPS J.* **12**, 11–26 (2010).
8. Kertesz, V. *et al.* Comparison of drug distribution images from whole-body thin tissue sections obtained using desorption electrospray ionization tandem mass spectrometry and autoradiography. *Anal. Chem.* **80**, 5168–5177 (2008).
9. Cecchelli, R. *et al.* Modelling of the blood-brain barrier in drug discovery and development. *Nat. Rev. Drug Discov.* **6**, 650–661 (2007).
10. Jeffrey, P. & Summerfield, S. Assessment of the blood-brain barrier in CNS drug discovery. *Neurobiol. Dis.* **37**, 33–37 (2010).
11. Mehdipour, A. R. & Hamidi, M. Brain drug targeting: a computational approach for overcoming blood-brain barrier. *Drug Discov. Today* **14**, 1030–1036 (2009).
12. Wager, T. T., Hou, X., Verhoest, P. R. & Villalobos, A. Moving beyond rules: the development of a central nervous system multiparameter optimization (CNS MPO) approach to enable alignment of druglike properties. *ACS Chem. Neurosci.* **1**, 435–449 (2010).
13. Prideaux, B. *et al.* High-sensitivity MALDI-MRM-MS imaging of moxifloxacin distribution in tuberculosis-infected rabbit lungs and granulomatous lesions. *Anal. Chem.* **83**, 2112–2118 (2011).
14. James, A. D.-P. A, Scott, G. & Zhao, J. Y. MALDI molecular imaging: Optimization of experimental techniques and applications in drug distribution studies. *Clin. Chem.* **51**, A204–205 (2005).
15. Sugiura, Y. & Setou, M. Imaging mass spectrometry for visualization of drug and endogenous metabolite distribution: toward in situ pharmacometabolomes. *JNIP* **5**, 31–43 (2010).
16. Nuttall, A. L. Techniques for the observation and measurement of red blood cell velocity in vessels of the guinea pig cochlea. *Hear. Res.* **27**, 111–119 (1987).
17. Blauth, C. I., Arnold, J. V., Schulenberg, W. E., McCartney, A. C. & Taylor, K. M. Cerebral microembolism during cardiopulmonary bypass. Retinal microvascular studies in vivo with fluorescein angiography. *Journal Thorac. Cardiovasc. Surg.* **95**, 668–676 (1988).
18. Saunders, N. R., Daneman, R., Dziegielewska, K. M. & Liddelow, S. A. Transporters of the blood-brain and blood-CSF interfaces in development and in the adult. *Mol. Aspects Med.* **34**, 742–752 (2013).
19. Wymann, M. P., Zvelebil, M. & Laffargue, M. Phosphoinositide 3-kinase signalling--which way to target? *Trends Pharmacol. Sci.* **24**, 366–376 (2003).
20. Liu, P., Cheng, H., Roberts, T. M. & Zhao, J. J. Targeting the phosphoinositide 3-kinase pathway in cancer. *Nat. Rev. Drug Discov.* **8**, 627–644 (2009).
21. Maira, S. M. *et al.* Identification and characterization of NVP-BKM120, an orally available pan-class I PI3-kinase inhibitor. *Mol. Cancer Ther.* **11**, 317–328 (2012).
22. Hagerstrand, D. *et al.* PI3K/PTEN/Akt pathway status affects the sensitivity of high-grade glioma cell cultures to the insulin-like growth factor-1 receptor inhibitor NVP-AEW541. *Neuro-Oncol.* **12**, 967–975 (2010).
23. Rasheed, B. K., S., T. T., McLendon, R. E., Parsons, R., Friedman, A. H., Friedman, H. S., Bigner, D. D. & Bigner, S. H. PTEN gene mutations are seen in high-grade but not in low-grade gliomas. *Cancer Res.* **57**, 967–975 (1997).
24. Wong, K. K. Recent developments in anti-cancer agents targeting the Ras/Raf/MEK/ERK pathway. *Recent Pat. Anticancer Drug Discov.* **4**, 28–35 (2009).
25. C, G.-E. Protein and lipid kinase inhibitors as targeted anticancer agents of the Ras/Raf/MEK and PI3K/PKB pathways. *Recent Pat. Anticancer Drug Discov.* **5**, 117–125 (2009).
26. Pfister, S. *et al.* BRAF gene duplication constitutes a mechanism of MAPK pathway activation in low-grade astrocytomas. *J. Clin. Invest.* 118, 1739–1749 (2008).
27. Jain, R. K. Normalizing tumor vasculature with anti-angiogenic therapy: a new paradigm for combination therapy. *Nat. Med.* **7**, 987–989 (2001).
28. Schneider, S. W., Ludwig, T., T., L., Braune, S., Oberleithner, H., Senner, V. & Paulus, W. Glioblastoma cells release factors that disrupt blood-brain barrier features. *Acta Neuropathol.* **107**, 272–276 (2004).
29. Haas-Kogan, D. A. *et al.* Epidermal growth factor receptor, protein kinase B/Akt, and glioma response to erlotinib. *J. Natl. Cancer Inst.* **97**, 880–887 (2005).
30. Shepherd, F. A. *et al.* Erlotinib in previously treated non-small-cell lung cancer. *N. Engl. J. Med.* **353**, 123–132 (2005).
31. Tang, P. A., Tsao, M. S. & Moore, M. J. A review of erlotinib and its clinical use. *EOP* **7**, 177–193 (2006).
32. Broniscer, A. *et al.* Plasma and cerebrospinal fluid pharmacokinetics of erlotinib and its active metabolite OSI-420. *Clin. Cancer Res.* **13**, 1511–1515 (2007).
33. Deeken, J. F. & Loscher, W. The blood-brain barrier and cancer: transporters, treatment, and Trojan horses. *Clin. Cancer Res.* **13**, 1663–1674 (2007).
34. Signor, L. *et al.* Analysis of erlotinib and its metabolites in rat tissue sections by MALDI quadrupole time-of-flight mass spectrometry. *J. Mass Spectrom.* **42**, 900–909 (2007).
35. Ling, J. *et al.* Metabolism and excretion of erlotinib, a small molecule inhibitor of epidermal growth factor receptor tyrosine kinase, in healthy male volunteers. Drug Metab. *Dispos.* **34**, 420–426 (2006).
36. Caravatti, P. A. M. The 'infinity cell': A new trapped-ion cell with radiofrequency covered trapping electrodes for fourier transform ion cyclotron resonance mass spectrometry. *Org. Mass Spectrom.* **26**, 514–518 (1991).
37. Karabacak, N. M., Easterling, M. L., Agar, N. Y. & Agar, J. N. Transformative effects of higher magnetic field in Fourier transform ion cyclotron resonance mass spectrometry. *J. Am. Soc. Mass Spectrom.* **21**, 1218–1222 (2010).
38. Caravatti, P. (ed. U.S. Patent, Ed.; Spectrospin AG, Switzerland; 1990).
39. Li, L. *et al.* A hierarchical algorithm for calculating the isotopic fine structures of molecules. *J. Am. Soc. Mass Spectrom.* **19**, 1867–1874 (2008).

Acknowledgments

This work was funded in part by US National Institute of Health (NIH) Director's New Innovator Award (1DP2OD007383-01 to N.Y.R.A.), and the NIH-NCI (P01 CA142536 to C.D.S. and N.Y.R.A.). The work received support from the Pediatric Low Grade Astrocytoma Program at Dana-Farber Cancer Institute, the Brain Science Foundation and the Daniel E. Ponton fund for the Neurosciences at BWH and the Dana-Farber/Novartis Program in Drug Discovery. J.N.A. received support from the Amyotrophic Lateral Sclerosis Association grant number 1856. We thank Daniel Feldman for his assistance with the tandem MS experiments.

Author contributions

N.Y.R.A., C.D.S., X.L., conceived and designed experiments, and wrote the manuscript. X.L. did the majority of the mass spectrometry imaging and all fluorescence imaging and data analysis. J.L.I. and X.L. performed tissue sectioning, staining, microscopy, data analysis, and contributed to manuscript preparation, and I.N. contributed computational expertise for mass spectrometry and microscopy data handling and analysis. M.E. assisted with tissue sectioning and 3D volume reconstruction. S.K., and C.M.S. contributed to preparation of the erlotinib experiments. L.Y.W., E.D., and J.A. prepared the animals for fluorescein and FITC imaging. K.A.K., M.L.E., J.N.A., and N.Y.R.A. conceived and performed the erlotinib experiments, imaging, and data analysis/interpretation. M.A.M. guided the preparation and dosing of animals for the BKM120 and RAF265 experiments. S.S. provided with neuropathology evaluation of tissue. D.D.S. contributed to experimental design and editing of the manuscript.

Additional information

Supplementary information accompanies this paper at http://www.nature.com/scientificreports

Competing financial interests: D.D.S. is an employee of Novartis, M.L.E. and K.A.K. are employees of Bruker Daltonics. In compliance with Harvard Medical School and Dana-Farber Cancer Institute guidelines on potential conflict of interest, C.D.S. is a consultant to Novartis.

How to cite this article: Liu, X. *et al.* Molecular imaging of drug transit through the blood-brain barrier with MALDI mass spectrometry imaging. *Sci. Rep.* **3**, 2859; DOI:10.1038/srep02859 (2013).